SWNTs. We have also investigated the effects of NO_2 and NH_3 on the electrical properties of mats of SWNT ropes made from as-grown laser ablation materials. In a 200-ppm NO_2 flow, the resistance of an SWNT mat is found to decrease from $R = 150$ to 80 ohms ($R_{before}/R_{after} \sim 2$) in ~10 min (Fig. 4A). In a 1% NH_3 flow, the resistance of a second SWNT mat increases from 120 to 170 ohms ($R_{after}/R_{before} \sim 1.5$) in ~10 min (Fig. 4B). In these bulk SWNT samples, the molecular interaction effects are averaged over metallic and semiconducting tubes. Also, the inner tubes in SWNT ropes are blocked from interacting with NO_2 and NH_3 because the molecules are not expected to intercalate into SWNT ropes. This explains the small resistance change of bulk SWNT mats by gas exposure compared to that of an individual S-SWNT.

The main feature of individual S-SWNT sensors, besides their small sizes, is that they operate at room temperature with sensitivity as high as 10^3. An individual nanotube sensor can be used to detect different types of molecules. The selectivity is achieved by adjusting the electrical gate to set the S-SWNT sample in an initial conducting or insulating state. The fast response of a nanotube sensor can be attributed to the full exposure of the nanotube surface area to chemical environments. Thus, nanotube molecular wires should be promising for advanced miniaturized chemical sensors.

References and Notes

1. M. S. Dresselhaus, G. Dresselhaus, P. C. Eklund, *Science of Fullerenes and Carbon Nanotubes* (Academic Press, San Diego, CA, 1996).
2. H. Dai, J. H. Hafner, A. G. Rinzler, D. T. Colbert, R. E. Smalley, *Nature* **384**, 147 (1996).
3. S. Wong, E. Joselevich, A. Woolley, C. Cheung, C. Lieber, *Nature* **394**, 52 (1998).
4. W. A. de Heer, A. Chatelain, D. Ugarte, *Science* **270**, 1179 (1995).
5. R. H. Baughman *et al.*, *Science* **284**, 1340 (1999).
6. S. Tans, A. Verschueren, C. Dekker, *Nature* **393**, 49 (1998).
7. Special issue on Gas-Sensing Materials, *MRS Bull.* **24** (1999).
8. Y. Shimizu and M. Egashira, *MRS Bull.* **24**, 18 (1999).
9. Y. Takao, K. Miyazaki, Y. Shimizu, M. Egashira, *J. Electrochem. Soc.* **141**, 1028 (1994).
10. H. M. McConnell *et al.*, *Science* **257**, 1906 (1992).
11. A. Mandelis and C. Christofides, *Physics, Chemistry and Technology of Solid State Gas Sensor Devices* (Wiley, New York, 1993).
12. J. Miasik, A. Hooper, B. Tofield, *J. Chem. Soc. Faraday Trans. 1* **82**, 1117 (1986).
13. S. Capone, S. Mongelli, R. Rella, P. Siciliano, L. Valli, *Langmuir* **15**, 1748 (1999).
14. M. C. Longergan *et al.*, *Chem. Mater.* **8**, 2298 (1996).
15. R. Martel, T. Schmidt, H. R. Shea, T. Hertel, P. Avouris, *Appl. Phys. Lett.* **73**, 2447 (1998).
16. T. Soh *et al.*, *Appl. Phys. Lett.* **75**, 627 (1999).
17. J. Kong, H. Soh, C. F. Quate, H. Dai, *Nature* **395**, 878 (1998).
18. G. Sberveglieri, S. Groppelli, P. Nelli, *Sens. Actuators B4*, 457 (1991).
19. C. Zhou, J. Kong, H. Dai, in preparation.
20. S. Peng and K. Cho, in preparation.
21. M. L. Hair, *Infrared Spectroscopy in Surface Chemistry* (Dekker, New York, 1967).
22. A. Cheng and W. A. Steele, *J. Chem. Phys.* **92**, 3867 (1990).
23. P. Sjovall, S. K. So, B. Kasemo, R. Franchy, W. Ho, *Chem. Phys. Lett.* **172**, 125 (1990).
24. P. Rowntree, G. Scoles, J. Xu, *J. Chem. Phys.* **92**, 3853 (1990).
25. P. A. Heiney, *J. Phys. Chem. Solids* **53**, 1333 (1992).
26. R. S. Lee, H. J. Kim, J. E. Fischer, A. Thess, R. E. Smalley, *Nature* **388**, 255 (1997).
27. L. Grigorian *et al.*, *Phys. Rev. Lett.* **80**, 5560 (1998).
28. We thank J. Han, L. Yang, and M. Tang for discussions.

Single-File Diffusion of Colloids in One-Dimensional Channels

Q.-H. Wei,*† C. Bechinger,* P. Leiderer

Single-file diffusion, prevalent in many processes, refers to the restricted motion of interacting particles in narrow micropores with the mutual passage excluded. A single-filing system was developed by confining colloidal spheres in one-dimensional circular channels of micrometer scale. Optical video microscopy study shows evidence that the particle self-diffusion is non-Fickian for long periods of time. In particular, the distribution of particle displacement is a Gaussian function.

Single-file diffusion (SFD) occurs when the individual pores of the medium are so narrow that the particles are unable to pass each other (*1, 2*). The sequence of particles remains unchanged over time, and thus, the basic principle of diffusion as a physical mixing process comes into question. The concept of SFD was originally introduced more than 40 years ago in biophysics to account for the transport of water and ions through molecular-sized channels in membranes (*3*); since then, in addition to biological systems (*4, 5*), SFD is also discussed in the context of interaction of Markov chains in statistics (*6*), the transportation of adsorbate molecules through zeolites (*2*), and charge-carrier migration in one-dimensional (1D) polymer and superionic conductors (*7*). Furthermore, SFD is also related to surface growth phenomena through some mapping (*8*).

As the mutual passage of particles is prohibited in single-filing (SF) systems, the movements of individual particles are correlated, even at long time periods, because the displacement of a given particle over a long distance necessitates the motion of many other particles in the same direction. This correlation is reflected in the long-time behavior of the mean-square displacement (MSD), which has been predicted for an infinite system to be (*6, 7, 9–11*)

$$\langle \Delta x^2 \rangle = 2F\sqrt{t} \qquad (1)$$

Faculty of Physics, University of Konstanz, Postfach M676, D-78457 Konstanz, Germany.

*To whom correspondence should be addressed. E-mail: qwei+@pitt.edu (Q.-H.W.) and clemens.bechinger@uni-konstanz.de (C.B.)
†Present address: Department of Physics and Astronomy, University of Pittsburgh, Pittsburgh, PA 15260, USA.

where F is the SF mobility and t is time. Accordingly, SFD processes, in contrast to 2D and 3D self-diffusion seen in colloidal systems (*12*), cannot be described by a diffusion coefficient; that is, the SFD does not obey Fick's laws.

Experimental evidence confirming non-Fickian behavior was unavailable for a long time because of the lack of ideal experimentally accessible SF systems. Recently, measurements of SFD became feasible in artificial crystalline zeolites. Adsorbate molecules, like methane or CF_4 with diameters of 3.8 and 4.7 Å, respectively, confined in $AlPO_4-5$ zeolite with a pore size of 7.3 Å, are considered to be good realizations of SF systems. Although some experimental evidence for the occurrence of SFD was found by pulsed field gradient nuclear magnetic resonance study (*13, 14*), some results from different groups and experimental methods are still in contradiction, even for the same system (*15, 16*), as indicated by Hahn and Kärger (*17*), who suggest and explore several possible reasons. Other effects, such as attractive particle interaction (*18*), the possible existence of correlations between particles of neighboring pores (*19*), have also been shown to play a vital role in the mechanism and rates of intracrystalline diffusion. Because of the shortage of structural information on the atomic level, the mechanism of molecular diffusion in zeolites, however, is still under debate.

We created a well-defined SFD model system by confining paramagnetic colloidal spheres of several micrometers in a set of circular trenches fabricated by photolithography. The channels are well-characterized, and the particle-particle interaction can be precisely adjusted by an external magnetic field. Moreover, because the time and length scales in such a colloidal system are easily accessed

Fig. 1. (**A**) Scanning electron microscope image of the 1D trenches fabricated on the photoresist polymer film by photolithography. (**B**) Optical microscope image of three concentric circular channels with colloidal particles confined in them (the small black objects inside the channels). After the cell was assembled, the colloidal particles sedimented to the bottom plate under the action of gravitation and were trapped in the microchannels (promoted by slightly tilting the substrate). With a particle density of 1.20 g cm^{-3}, the gravitation potential well of the 5-μm-deep channel is ~400$k_B T$ in depth. After most of the particles were trapped in the channels, the sample was carefully adjusted to horizontal before the experiments. The dynamics of colloidal particles was monitored with a home-built inverted transmission optical microscope system that was connected to a charge-coupled device camera and a computer.
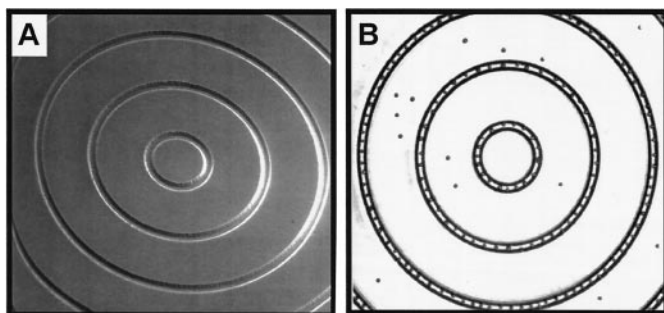

Fig. 2. (**A**) Typical trajectories for eight neighboring particles in the largest channel in Fig. 1A. The instantaneous particle coordinates were extracted from digitized pictures with an image-processing algorithm and saved in a computer for later analysis. From those data, we obtained the particle trajectories. The system was equilibrated for at least 4 hours before each measurement. To obtain the long-time behavior, we recorded the coordinates of colloidal particles for ~8 hours, with a time interval of ~8 s between two adjacent pictures. (**B**) Log-log plot of the measured particle MSDs versus the observation time for five different particle interaction strengths Γ: 0.66, open circles; 1.1, solid circles; 2.34, open squares; 4.03, solid triangles; and 7.42, open triangles. The data points have been shifted upward by ln 2 for clarity, and the solid lines are best fit with Eq. 1 with the mobility F as an adjustable parameter.
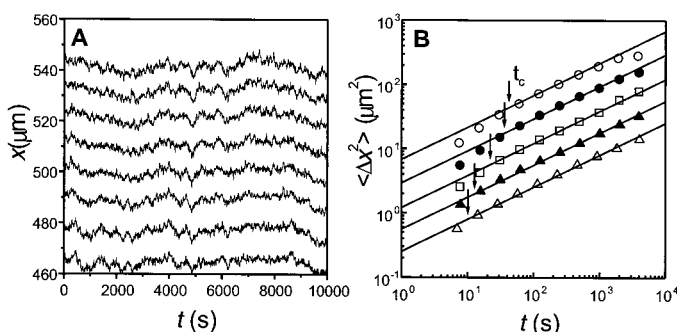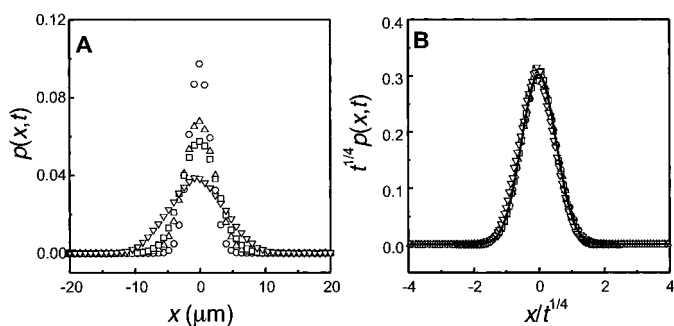

Fig. 3. (**A**) The particle displacement distribution function $p(x, t)$ for $\Gamma = 4$ at different times t: 77 s, circles; 385 s, triangles; 770 s, squares; and 3850 s, inverted triangles. (**B**) The distribution function $p(x, t)$ of (A) replotted by scaling $p(x, t) \to t^{1/4} p(x, t)$, $x \to x/t^{1/4}$. The solid curve is a Gaussian fit with Eq. 2, with the fitting parameter $F = 0.14$ μm/s$^{1/2}$.

way). The particles were doped with Fe_2O_3 clusters and are paramagnetic. Thus, when an external magnetic field is applied perpendicular to the sample plane, a magnetic dipole moment M is induced in the colloids (which is proportional to the weak field strengths B that we used) that gives rise to a repulsive pair interaction potential of the form $V(r) = (\mu_0/4\pi)M^2(B)r^{-3}$, where r is the particle distance and μ_0 is the vacuum permeability. In order to characterize the interaction strength between particles, we introduce the quantity $\Gamma = \beta(\mu_0/4\pi)\chi_{eff}^2 B^2 R^{-3}$, which is the mean interaction energy normalized by the thermal energy $1/\beta = k_B T$, where k_B is the Boltzmann constant and T is the temperature. Here, R is the mean particle distance, and χ_{eff} is the magnetic susceptibility of the particles, which was determined to be 2.2×10^{-12} A m^2 T^{-1} (20). The particle-wall interaction can be considered as a hard sphere-wall interaction to a good approximation.

A typical real-space configuration of the particles at $\Gamma = 4$ is shown in Fig. 1B. Each channel appears as two closely spaced concentric rings because of the diffraction of the light at its walls into the photoresist. The particles are the dark objects within the channels. Most of the particles are trapped in the channels, whereas only a few reside on the elevated areas and do not influence the diffusion behavior of particles in the channels. The channels are narrow enough to meet the SF condition and prohibit the mutual passage of particles.

In Fig. 2A, we plotted typical trajectories of eight neighboring particles obtained at $\Gamma = 4$ from the largest channel in Fig. 1B. The particle position x corresponds to their angular coordinate multiplied by the channel radius. As can be seen, the trajectories never cross during the measuring time, which indicates that the SF condition is satisfied. The correlation of particle positions for long periods of time, as a characteristic of SFD, can also be seen from Fig. 2A.

The results of MSD in a log-log plot for five different magnetic field strengths ($\Gamma = 0.66$, 1.10, 2.34, 4.03, and 7.42) are shown in Fig. 2B. For the calculation of MSD, we averaged over both the time t and all of the particles in the channel, or $\langle \Delta x^2 \rangle = \Sigma_i \langle [x_i(t + t') - x_i(t')]^2 \rangle_{t'}/N$, where N is the total number of particles and i is the particle index. The solid lines in Fig. 2B correspond to the best fits according to Eq. 1 with the mobility F as the only adjustable parameter. The predicted $t^{1/2}$ behavior was seen over more than two decades of time. The small deviations from the solid lines at small time scales correspond to the crossover between the long-time and short-time diffusion of the particles. The crossover time t_c (arrows in Fig. 2B) is significantly shifted to larger values when the magnetic dipole repulsion between the particles decreases.

We also calculated the distribution function of displacements $p(x, t)$, which is defined

with video microscopy, the trajectories of individual particles can be followed over long periods of time. We unambiguously observed the non-Fickian behavior of SFD and confirm the theoretically predicted Gaussian distribution of particle displacements.

The sample cell was composed of two optical flats separated by an O ring of 0.5-mm thickness. The bottom plate was first coated with a thin layer of poly(methyl methacrylate) to prevent colloidal particles from sticking to the glass surface. On top of this film, a 5-μm-

thick layer of a transparent photoresist was deposited. Afterward, a set of concentric circular channels (7 μm in width and 33 to 1608 μm in diameter) was etched into the photoresist by means of photolithography (Fig. 1A). The distance between adjacent channels, 63 μm, is much larger than the mean particle separation (11 μm), which rules out correlation between particles in neighboring channels.

We used an aqueous suspension of paramagnetic polystyrene colloids with a diameter of 3.6 μm (M-350 Dyno AS, Lillestroem, Nor-
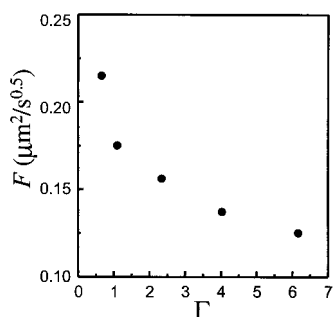
Fig. 4. The single-file particle mobility obtained from the fittings shown in Fig. 2B as a function of the normalized particle interaction strength Γ.

as the conditional probability of finding a particle at position x after time t with the particle located for $t = 0$ at $x = 0$. In Fig. 3A, we show the result of $p(x, t)$ for $\Gamma = 4$ at four different times, which are all greater than t_c. Self-diffusion of particles causes $p(x, t)$ to broaden with time.

Despite the simplicity of the physical situation describing SF conditions, theoretical treatment remains a highly sophisticated task. Analytical results are only obtained for long time limits for hard rods hopping in an infinite 1D lattice (called a 1D exclusion model). It has been predicted that $p(x, t)$ follows (6, 10, 14)

$$p(x, t) \; = \; \frac{1}{\sqrt{4\pi F t^{1/4}}} \exp(-x^2/4Ft^{1/2}) \quad (2)$$

This form, however, is suggested to remain valid under more general conditions whenever the SF effect is important.

To compare our data with Eq. 2, we re-plotted the data of Fig. 3A in Fig. 3B; all of the data points collapse to a master curve after a rescaling of the axis. In addition, a Gaussian function fit (Fig. 3B, solid curve) shows good agreement with the data. From the only adjustable parameter of the Gaussian fit, the SF mobility can be derived, which is in agreement with the value obtained from the MSD data. This observation is also true for the $p(x, t)$ for the other magnetic fields. It should be emphasized that Eq. 2 has not been directly observed in experiments before.

The 1D exclusion model predicts that F decreases with the particle density ρ according to $F \propto (1 - \rho)/\rho$. In our system, however, it is more convenient to change the particle interaction strength Γ while keeping the particle density constant. This change is equivalent to changing the particle density because an increase in Γ results in an increase of collision rates between particles or, equivalently, an increase in particle density. The measured mobility (Fig. 4) decreases with the increase of particle interaction energy, which is qualitatively in agreement with the theoretical prediction.

However, unlike the hard-rod interaction in the theoretical exclusion model, we have a long-range pair interaction, and the hydrodynamic interactions caused by the particles moving in the surrounding fluid also play an important role. Therefore, detailed comparison with theory should take these two aspects into account.

References and Notes

1. E. J. Harris, *Transport and Accumulation in Biological Systems* (Butterworths Scientific, London, 1960); B. Alberts *et al.*, *Molecular Biology of the Cell* (Garland, New York, 1994).
2. J. Kärger and D. M. Ruthven, *Diffusion in Zeolites and Other Microporous Solids* (Wiley, New York, 1992); N. Y. Chen, T. F. Degnan, C. M. Smith, *Molecular Transport and Reaction in Zeolites* (VCH, New York, 1994).
3. A. L. Hodgkin and R. D. Kenes, *J. Physiol. (London)* **128**, 61 (1955).
4. E. J. A. Lea, *J. Theor. Biol.* **5**, 102 (1963); H. Rickert, *Z. Phys. Chem. Neue. Folge.* **43**, 129 (1964); D. G. Levitt, *Biochim. Biophys. Acta* **373**, 115 (1974).
5. P. A. Rosenberg and A. Finkelstein, *J. Gen. Physiol.* **72**, 341 (1978); S. Draber, R. Schultze, U.-P. Hansen, *J. Membr. Biol.* **123**, 183 (1991); J. A. Hernandez and J. Fischbarg, *J. Gen. Physiol.* **99**, 645 (1992); T. Chou and D. Lohse, *Phys. Rev. Lett.* **82**, 3552 (1999).
6. R. Arratia, *Ann. Probab.* **11**, 362 (1983).
7. P. M. Richards, *Phys. Rev. B* **16**, 1393 (1977); P. A. Fedders, *Phys. Rev. B* **17**, 40 (1978).
8. T. Halpin-Healy and Y. C. Zhang, *Phys. Rep.* **254**, 215 (1995).
9. S. Alexander and P. Pincus, *Phys. Rev. B* **18**, 2011 (1978).
10. H. van Beijeren, K. W. Kehr, R. Kutner, *Phys. Rev. B* **28**, 5711 (1983).
11. J. Kärger, *Phys. Rev. A* **45**, 4173 (1992); *Phys. Rev. E* **47**, 1427 (1993); K. Hahn and J. Kärger, *J. Phys. A Math. Gen.* **28**, 3061 (1995).
12. G. Nägle, *Phys. Rep.* **272**, 215 (1996); X. Qiu, H. D. Ou-Yang, P. M. Chaikin, *J. Phys. (Paris)* **49**, 1043 (1988); A. van Blaaderen, J. Peetermans, G. Maret, J. K. G. Dhont, *J. Chem. Phys.* **96**, 4591 (1992).
13. V. Gupta *et al.*, *Chem. Phys. Lett.* **247**, 596 (1995).
14. V. Kukla *et al.*, *Science* **272**, 702 (1996); K. Hahn, J. Kärger, V. Kukla, *Phys. Rev. Lett.* **76**, 2762 (1996).
15. S. S. Nivarthi, A. V. McCormick, H. T. Davis, *Chem. Phys. Lett.* **229**, 197 (1994).
16. H. Jobic *et al.*, *J. Phys. Chem. B* **101**, 5834 (1997).
17. K. Hahn and J. Kärger, *J. Phys. Chem. B* **102**, 5766 (1998).
18. D. S. Sholl and K. A. Fichthorn, *Phys. Rev. Lett.* **79**, 3569 (1997).
19. R. Radhakrishnan and K. Gubbins, *Phys. Rev. Lett.* **79**, 2847 (1997).
20. K. Zahn, thesis, University of Strasbourg, Strasbourg, France (1997).
21. We thank K. Zahn for giving us the paramagnetic colloidal particles. The work is supported by Deutsche Forschungsgemeinschaft through grant SFB513.

Three-Dimensional Direct Imaging of Structural Relaxation Near the Colloidal Glass Transition

Eric R. Weeks,[1]* J. C. Crocker,[2] Andrew C. Levitt,[2] Andrew Schofield,[3] D. A. Weitz[1]

Confocal microscopy was used to directly observe three-dimensional dynamics of particles in colloidal supercooled fluids and colloidal glasses. The fastest particles moved cooperatively; connected clusters of these mobile particles could be identified; and the cluster size distribution, structure, and dynamics were investigated. The characteristic cluster size grew markedly in the supercooled fluid as the glass transition was approached, in agreement with computer simulations; at the glass transition, however, there was a sudden drop in their size. The clusters of fast-moving particles were largest near the α-relaxation time scale for supercooled colloidal fluids, but were also present, albeit with a markedly different nature, at shorter β-relaxation time scales, in both supercooled fluid and glass colloidal phases.

As a glass-forming liquid is cooled, its viscosity smoothly but rapidly increases by many orders of magnitude (1–4). This macroscopic viscosity divergence is related to the divergence of the microscopic structural relaxation time (α-relaxation time). Microscopically, a glass still has liquid-like structure; no structural change has been found which would explain the glass transition (3–5). Instead, theories for the glass transition focus on microscopic dynamical mechanisms (1–4, 6–8). The underlying concept of many of these theories is the Adam and Gibbs hypothesis (6), which states that flow in a supercooled fluid involves cooperative motion of

---

[1]Department of Physics and Division of Engineering and Applied Sciences, Harvard University, Cambridge, MA 02138, USA. [2]Department of Physics and Astronomy, University of Pennsylvania, Philadelphia, PA 19104, USA. [3]Department of Physics and Astronomy, University of Edinburgh, Edinburgh, Scotland EH9 3JZ, UK.

*To whom correspondence should be addressed. E-mail: weeks@deas.harvard.edu